**Biogeosciences**
Discussions

Open Access

# What prevents nitrogen depletion in the OMZ of the Eastern Tropical South Pacific?

## B. Su, M. Pahlow, H. Wagner, and A. Oschlies

GEOMAR Helmholtz-Zentrum für Ozeanforschung Kiel, Marine Biogeochemical Modelling, Düsternbrooker Weg 20, 24105 Kiel, Germany

Correspondence to: B. Su (bsu@geomar.de)

Discussion Paper | Discussion Paper | Discussion Paper | Discussion Paper |

BGD
11, 11095–11138, 2014

What prevents nitrogen depletion in the OMZ of the Eastern Tropical South Pacific?

B. Su et al.

Title Page

Abstract | Introduction
Conclusions | References
Tables | Figures

◄◄ | ►►
◄ | ►

Back | Close

Full Screen / Esc

Printer-friendly Version

Interactive Discussion

## Abstract

Local coupling between nitrogen fixation and denitrification in current biogeochemical models could result in a run-away feedback in open-ocean oxygen minimum zones (OMZs), eventually stripping OMZ waters of all fixed nitrogen. This feedback does not seem to operate at full strength in the ocean, as nitrate does not generally become depleted in open-ocean OMZs. To explore in detail the mechanism that prevents nitrogen depletion in the OMZ of the Eastern Tropical South Pacific (ETSP), we develop a box model with fully prognostic cycles of carbon, nutrients, and oxygen in the upwelling region and its adjacent open ocean. Ocean circulation is calibrated with $\Delta^{14}C$ data of the ETSP. The sensitivity of the simulated nitrogen cycle to nutrient and oxygen exchange and ventilation from outside the model domain and remineralization scales inside an OMZ is analysed. For the entire range of model configurations explored, we find that the fixed-N inventory can be stabilized at non-zero levels in the ETSP OMZ only if the remineralization rate via denitrification is slower than that via aerobic respiration. In our optimum model configuration, lateral oxygen supply to the model domain required at rates sufficient to oxidize at least about a fifth of the export production in the model domain to prevent anoxia in the deep ocean. Under these conditions, our model is in line with the view of phosphate as the ultimate limiting nutrient for phytoplankton, and implies that for the current notion of nitrogen fixation being favored in N-deficit waters, the water column of the ETSP could even be a small net source of fixed-N.

## 1  Introduction

The oceanic fixed nitrogen (fixed-N) budget is an essential control on the potential of the ocean to sequester atmospheric $CO_2$ via the marine biological pump. Denitrification is generally recognized as a major loss of fixed nitrogen, whereas the balance of the global oceanic nitrogen budget remains controversial. Accordingly, estimates for the global oceanic fixed-N budget range from sources roughly balancing sinks (Gruber

B. Su et al.

and Sarmiento, 1997; Gruber, 2004; Eugster and Gruber, 2012) to a rather large net deficit between 140 and 234 Tg N yr$^{-1}$ (Codispoti et al., 2001; Galloway et al., 2004; Codispoti, 2007).

One of the main uncertainties in the global marine nitrogen budget is the extent of nitrogen loss via denitrification and anaerobic ammonium oxidation (anammox) in oxygen minimum zones (OMZs), located in tropical coastal upwelling regions. Coastal upwelling zones are often associated with very high primary production. Subsequent decomposition of sinking organic matter leads to high levels of oxygen consumption in subsurface waters. Under conditions of sluggish circulation, oxygen-poor source waters, or lack of exchange with oxygenated surface waters, OMZs can develop, usually at intermediate depths of about 200–700 m (Bethoux, 1989; Capone and Knapp, 2007). An OMZ is commonly defined as a water body with an $O_2$ concentration below 20 µmol L$^{-1}$ (Paulmier and Ruiz-Pino, 2009). The four major open-ocean OMZs are in the Eastern North Pacific (ENP), the Eastern Tropical South Pacific (ETSP), the Arabian Sea, and the Bay of Bengal. OMZs currently account for only about 8 % of the global ocean area but are thought to be responsible for 30–50 % of the total fixed-N loss (Gruber and Sarmiento, 1997; Codispoti et al., 2001; Dalsgaard et al., 2005; Paulmier and Ruiz-Pino, 2009).

Canfield (2006) used a simple steady-state box model of a coastal OMZ to show that a positive feedback between $N_2$ fixation and denitrification could strip the OMZ of all fixed nitrogen when $N_2$ fixation was permitted to restore the nitrate : phosphate ratio to Redfield proportions in the surface ocean. Observed concentrations of fixed-N (nitrate plus nitrite) in OMZ waters, however, typically range from about 15 to 40 µmol L$^{-1}$ (Codispoti and Richards, 1976; Codispoti and Packard, 1980; Morrison et al., 1998; Voss et al., 2001). A possible explanation for the relatively high nitrate concentrations even in the suboxic core of open-ocean OMZs could be low levels of nitrogen fixation in the overlying surface waters (Landolfi et al., 2013). However, recent interpretations of observed fixed-N deficits relative to the Redfield equivalent of phosphorus point to high rates of nitrogen fixation closely related to the upwelling of nitrogen-deficit waters along

B. Su et al.

the South American coast (Deutsch et al., 2007). Although alternative explanations for these nutrient patterns have been proposed (Mills and Arrigo, 2010), direct measurements have confirmed the occurrence of nitrogen fixation in and above the OMZ of the ETSP (Fernandez et al., 2011). Global biogeochemical models also generally predict substantial rates of $N_2$ fixation in the nitrate-deficit waters of the upwelling region of the ETSP that, if not compensated by some ad-hoc slow-down of remineralization in suboxic conditions, lead to a complete draw-down of nitrate in the OMZ (Moore and Doney, 2007; Schmittner et al., 2008). The question of how non-zero nitrate concentrations can be maintained in the OMZ thus still awaits a mechanistic answer.

The computational efficiency of box models makes them suitable for sensitivity analysis requiring thousands of model evaluations. In spite of its simplicity, Canfield's (2006) box model is also able to capture the most important first-order interactions among ocean circulation, nitrogen fixation, denitrification, and OMZs. However, Canfield's model was limited in its power to investigate the influence of open ocean nutrients and oxygen conditions on the upwelling region, because its dynamics were restricted to the OMZ, where all biogeochemical tracers were prescribed in the surrounding waters. Based on Canfield's (2006) steady-state formulation with prescribed oxygen and nutrient concentrations at all depths outside the OMZ, we here present a fully prognostic box model of $NO_3^-$, $PO_4^{3-}$ and $O_2$ cycles in a coastal upwelling region and an adjacent ocean basin. We employ this model to examine under which conditions the observed situation of an essentially complete drawdown of subsurface oxygen and an incomplete drawdown of nitrate can be reproduced for the case of the ETSP. Sensitivity experiments explore how nutrient exchange and oxygen ventilation from the southern boundary influence the nitrogen budget within the model domain.

By including a prognostic description not only of conditions within the OMZ, but also in the water surrounding it, we aim to represent local as well as spatially-separated feedbacks between the relatively small OMZ and the much larger open-ocean basin. The model describes net primary and export production by ordinary and $N_2$-fixing phytoplankton, as well as aerobic and anaerobic remineralization. The latter is generally

associated with nitrogen loss, commonly attributed to denitrification (Codispoti, 1995). Anammox has recently been suggested as another major pathway for fixed-N removal (Kuypers et al., 2005; Hamersley et al., 2007; Molina and Farías, 2009), but the relative contributions of anammox and denitrification are still a matter of debate (Ward et al., 2009; Bulow et al., 2010). In our model, we do not explicitly resolve the different inorganic nitrogen species and pragmatically consider all loss of fixed-N via anaerobic remineralization as denitrification. In Canfield's (2006) model, most of the physical model parameters were constrained by observations from suboxic upwelling zones in the Arabian Sea and the Eastern Tropical North and South Pacific. The physical dynamics of our model system is governed by vertical and horizontal mixing and advection, which are calibrated with $\Delta^{14}$C data of the ETSP from GLODAP (Global Ocean Data Analysis Project, Key et al., 2004).

## 2  Model description

Figure 1 shows the model structure, consisting of five boxes representing an upwelling region and an adjacent ocean basin. The U box represents the upper upwelling region. The UM box is the underlying OMZ, where suboxia is expected to develop. The S box represents the surface ocean away from the upwelling zone. Below the S box sits the I box, which represents water of intermediate depth and exchanges water with UM. D is the deep box, which represents water deeper than 500 m. When the UM, I, or D boxes become suboxic, denitrification will ensue to remineralize the exported organic matter, causing a loss of fixed nitrogen (Denif).

Prognostic tracers represent $NO_3^-$, $PO_4^{3-}$, $O_2$, $^{14}$C and the biomass of ordinary and $N_2$-fixing phytoplankton, respectively (Table 1). The rate of concentration change of a tracer ($X_i$) in box $i$ is composed of physical transport, Transport($X_i$), and a sources-minus-sinks term, SMS($X_i$), which represents the effects of biotic processes, air–sea gas exchange and, in the case of $^{14}$C, radioactive decay on the tracer concentration

(Eq. 1).

$$\frac{dX_i}{dt} = \frac{\text{Transport}(X_i) + \text{SMS}(X_i)}{V_i} \quad i \in [U, S, UM, I, D] \tag{1}$$

where U, S, UM, I and D refer to the model boxes defined above and $V_i$ to the corresponding volumes (Fig. 1).

## 2.1 Transport model

Advection represents the large-scale circulation and is indicated in Fig. 1 by wide grey lines. $L_U$ and $L_S$ are the horizontal scales of the upwelling region and the open ocean, and $H_U$, $H_{UM}$ and $H_D$ refer to the thickness of the respective boxes. The volumes $V_i$ of the boxes are defined in this 2-D model by $V_i = H_i \cdot L_i$. $K_{US}$, $K_{UM}$ and $K_H$ are the coefficients of mixing between different boxes. $A$ and $B$ represent the deep and shallow large-scale circulation. The upwelling intensity into box U is given by $A + B$. The tracer transport equations for the standard configuration are given in Appendix A (Eqs. A1–A5). All parameters are defined in Tables 4 and 5.

## 2.2 Biogeochemical model

The ecological model is composed of two phytoplankton types, ordinary phytoplankton, Phy, and nitrogen fixers, NF. The SMS terms for phytoplankton are then obtained as the difference between net primary production (NPP) and mortality ($M$):

$$\text{SMS}(\text{Phy}_i) = (\text{NPP}^{\text{Phy}_i} - M^{\text{Phy}_i} \cdot \text{Phy}_i) \cdot V_i \quad i \in [U, S] \tag{2}$$

$$\text{SMS}(\text{NF}_i) = (\text{NPP}^{\text{NF}_i} - M^{\text{NF}_i} \cdot \text{NF}_i) \cdot V_i \quad i \in [U, S] \tag{3}$$

Both types require phosphate, whereas nitrate is required in addition to phosphate only by Phy, and NF can fix $N_2$ as long as $PO_4^{3-}$ is available. Growth of ordinary phytoplankton is described by a Liebig-type dependence on the nitrate and phosphate limitation

11100

terms (Eq. 4),

$$\text{NPP}^{\text{Phy}_i} = \mu \cdot \min\left(\frac{N_i}{N_i + N_h}, \frac{P_i}{P_i + P_h}\right) \cdot \text{Phy}_i \quad i \in [U, S] \tag{4}$$

$$\text{NPP}^{\text{NF}_i} = \mu_{\text{NF}} \cdot \frac{P_i}{P_i + P_h} \cdot \text{NF}_i \quad i \in [U, S] \tag{5}$$

where $i$ is the model box, $\mu$ and $\mu_{\text{NF}}$ are the maximum growth rates of $\text{Phy}_i$ and $\text{NF}_i$ respectively. $N_i$ and $P_i$ are nitrate and phosphate concentrations, and $N_h$ and $P_h$ are half-saturation concentrations for nitrate and phosphate.

$N_2$ fixers are given a lower maximum growth rate ($\mu_{\text{NF}}$, Eq. 5), which is 1/3 of the maximum growth rate of ordinary phytoplankton ($\mu$), to account for the high cost of nitrogen fixation (La Roche and Breitbarth, 2005). The dependence of NF on iron is not explicitly considered in this model (Mills et al., 2004). Both Phy and NF use nitrogen and phosphorus in the Redfield ratio of 16 : 1 (Redfield et al., 1963). Phytoplankton mortality can be linear or quadratic in Phy and NF depending on the model configuration. Sensitivity experiments are also performed with a configuration where $N_2$ fixation is inhibited by $\text{NO}_3^-$, but overall results are found to be virtually unchanged (Appendix D).

Dead phytoplankton is immediately remineralized in the surface layer and underlying boxes according to the respective remineralization fraction $f_i$ of box $i$. Remineralization occurs preferentially via aerobic respiration, with anaerobic remineralization and the associated nitrogen loss setting in only when all $O_2$ has been consumed by aerobic respiration. Phytoplankton growth and aerobic remineralization together with denitrification and, once all inorganic nitrogen is consumed, remineralization via sulfate reduction define the SMS terms of the nitrogen and phosphorus cycles:

$$\text{SMS}(N_i) = -\text{NPP}^{\text{Phy}_i} \cdot V_i + \text{Rem}_i^N - \text{Denif}_i \tag{6}$$

$$\text{SMS}(P_i) = -\frac{(\text{NPP}^{\text{Phy}_i} + \text{NPP}^{\text{NF}_i}) \cdot V_i}{r_p} + \text{Rem}_i^P \tag{7}$$

where the remineralization (Rem) and denitrification (Denif) terms are defined in Appendix B.

$O_2$ is set constant in the surface ocean boxes U and S, which are in immediate contact with the atmosphere, but varies as a function of transport and respiration in the UM, I and D boxes. Thus, the aerobic respiration terms ($Res_i$) are only needed in the interior boxes UM, I and D:

$$SMS(O_{2i}) = -Res_i \quad i \in [UM, I, D] \tag{8}$$

where Res is defined in Appendix B (Eq. B10). Note that aerobic respiration will, in general, also take place in anoxic model boxes, where it utilizes the $O_2$ transported from adjacent boxes, before anaerobic respiration starts. All model runs are initialized with $O_2$, $NO_3^-$ and $PO_4^{3-}$ annual data from the World Ocean Atlas 2009 (Garcia et al., 2010a, b), averaged over the regions indicated in Table 2.

## 2.3 Model calibration

In the present work, the prescribed transport among the different boxes in terms of advection and mixing was calibrated by fitting the modeled $\Delta^{14}C$ distribution to the GLO-DAP "pre-bomb" $\Delta^{14}C$ distribution of the Eastern Tropical South Pacific (Key et al., 2004; Table 2). The $^{13}C$ fractionation-corrected ratio of $^{14}C/^{12}C$, $\Delta^{14}C$, is commonly used in ocean modeling to evaluate and calibrate model physics (Toggweiler et al., 1989; Shaffer and Sarmiento, 1995), because it tends to cancel the effect of the biotic downward transport of $^{14}C$ with the rain of organic particles produced by marine organisms. The $\Delta^{14}C$ distribution in our model is simulated with the help of a water-mass tracer, $\widehat{\Delta^{14}C}$, which is converted to $\Delta^{14}C$ units as follows:

$$\Delta^{14}C = 1000(\widehat{\Delta^{14}C} - 1)\,‰ \tag{9}$$

The $^{14}C$ dynamics in the model includes input from the atmosphere at the sea surface and radioactive decay with decay rate $\lambda = 1.21 \times 10^{-4}\,yr^{-1}$ within the model domain.

The SMS term for $\widehat{\Delta^{14}C}$ is thus given by:

$$\text{SMS}(\widehat{\Delta^{14}C}_i) = \left(\frac{g_i(\widehat{\Delta^{14}C}_a - \widehat{\Delta^{14}C}_i)}{H_i} - \lambda\widehat{\Delta^{14}C}_i\right)\cdot V_i \quad i \in [\text{U, UM, S, I, D}] \tag{10}$$

where $\widehat{\Delta^{14}C}_i$ is the value of $\widehat{\Delta^{14}C}$ in box $i$, $\widehat{\Delta^{14}C}_a$ is atmospheric $\widehat{\Delta^{14}C}$, and the gas exchange rate $g_i = 0$ for $i \in [\text{UM, I, D}]$. We assume that the $\Delta^{14}C$ of the preindustrial atmosphere, $\Delta^{14}C_a$, is 0‰; therefore, the atmospheric $\widehat{\Delta^{14}C}_a$ is 1. Model configurations with an open southern boundary also include $^{14}C$ exchange with the adjacent subtropical ocean. We also investigate how sensitive our main conclusions are to the uncertainty in the $\Delta^{14}C$ data. Table 2 shows the $\Delta^{14}C$ values used for the calibrations of the different model configurations. Transport and SMS terms for $\overline{^{14}C}$ constitute a system of 5 linear equations in 7 parameters, including the transport parameters $A$, $B$, $K_{US}$, $K_{UM}$, $K_H$ and the air–sea $\overline{^{14}C}$ exchange coefficients for $g_U$ and $g_S$. After setting $g_U$ and $g_S$, the 5 equations can be inverted to solve for the transport parameters. A detailed description of the inversion scheme is provided in Appendix C.

## 2.4 Model configurations

Above transport and biogeochemical formulations define the standard (STD) configuration, where phytoplankton mortality is formulated by a linear term with constant coefficient ($M^{\text{Phy}_i} = M^{\text{NF}_i} = M$). In the STD configuration, the above transport and biogeochemical models are applied without exchange with the southern boundary. Fixed fractions $f_i$ of net primary production in U and S are remineralized in the U, UM, S and I boxes, with the remainder being remineralized in D (Fig. 1). Nutrient regeneration is assumed to be instantaneous.

In order to investigate the relationships between the different biotic and physical processes and the nitrogen cycle in an OMZ, we introduce eight additional model configurations (Table 3): (1) In the QM configuration, a quadratic form is adopted for the

mortality of both ordinary phytoplankton and nitrogen fixers:

$$M^{\mathrm{Phy}_i} = M_q \mathrm{Phy}_i \qquad M^{\mathrm{NF}_i} = M_q \mathrm{NF}_i \qquad (11)$$

Possible mechanisms represented by a quadratic mortality term are viral lysis, phytoplankton aggregation, or a feedback between zooplankton grazing and phytoplankton concentration. (2) In the Reduced-denitrification (RD) configuration, denitrification in the OMZ is reduced to 1/5 of the rate of the STD configuration following the procedure applied in the global biogeochemical circulation model by Schmittner et al. (2008). When oxygen is exhausted in the OMZ, denitrification within the UM box will then be responsible for only 1/5 of the remaining organic matter remineralization and the remainder will be remineralized in the D box (Eqs. B7 and B8). (3) The Ventilation-D (VD) configuration modifies the QM configuration in that the southern boundary of the model domain is partially opened to allow ventilation of $O_2$ and $^{14}C$ (but not $NO_3^-$ and $PO_4^{3-}$) to the D box from the southern subtropical ocean (Eq. A7). The circulation parameters were recalibrated to account for ventilation of $^{14}C$ from the south. Ventilation is simulated by applying lateral mixing with the subtropical oligotrophic ocean tracer reservoir with prescribed $^{14}C$ and $O_2$ concentrations inferred from observations. All other biogeochemical processes within the model domain are kept the same as in the QM configuration. (4) In the Ventilation-D + Reduced-denitrification (VDRD) configuration, the reduced denitrification rate is applied in the VD configuration. (5) In the Ventilation-ID (VID) configuration, the partially open southern boundary is extended to allow ventilation of $O_2$ and $^{14}C$ also into the I box from the subtropical ocean (Eq. A6). Again, circulation parameters are recalibrated against observed $\Delta^{14}C$ taking into account the $^{14}C$ exchange between the subtropical ocean and the I and D boxes. (6) In the Ventilation-ID + Reduced-denitrification (VIDRD) configuration, the reduced denitrification rate is also applied in the VID configuration. (7) In the Open-boundary (OB) configuration, nutrient mixing is added to the VID configuration to allow for exchange of nutrients between the I and D boxes and the subtropical ocean. (8) In the Open-boundary + Reduced-denitrification (OBRD) configuration, the reduced-denitrification

rate is again added to the OB configuration. The physical transports of $NO_3^-$ and $PO_4^{3-}$ for the I and D boxes in the last six configurations are represented by Eqs. (A6) and (A7) in Appendix A.

For the OBRD configuration, sensitivity experiments are performed in which the mix-
5  ing rates with the southern boundary, $K_H$, is reduced for individual tracers (nutrients, oxygen) or combinations thereof from full rates to zero. To explore the sensitivity with respect to the circulation parameters of the box model, simulations of the OBRD con-figuration were repeated with individual circulation parameters varied by ±10 %, ±20 % and ±50 %, respectively. The sensitivity of $NO_3^-$ and $O_2$ concentrations in the OMZ to
10  different physical parameters derived from variations of the $\Delta^{14}C$ data and $O_2$ concen-trations in the U-box is also examined.

## 3  Results

The physical circulation parameters calibrated with $\Delta^{14}C$ are given in Table 4. The resulting circulation is comparable with our expectations for the upwelling region of
15  the Eastern Tropical South Pacific. The parameters of the biogeochemical model are shown in Table 5.

### 3.1  Biogeochemical tracer concentrations

Nutrient and oxygen concentrations in the upwelling region (boxes U and UM) are in-fluenced by physical exchange with regions outside the upwelling zone (boxes I and D)
20  and subsequent remineralization of exported organic matter. In the STD configuration, $NO_3^-$ levels in the UM box are quickly exhausted by denitrification in the UM box (black bars in Fig. 2), where decomposition of exported organic matter consumes all $O_2$ enter-ing the UM box via advection and diffusion, and all $NO_3^-$ entering via physical transport and remineralization of exported organic matter. In the STD configuration, $O_2$ is also
25  depleted in the D box, owing to weak ventilation. This results in over 90 % of the initial

nitrate being lost from the model domain by denitrification once the model has reached steady state. The large nitrate deficit with respect to phosphate in the upwelling waters results in nitrogen fixers becoming dominant in the U box despite having a lower maximum growth rate than ordinary phytoplankton. Ordinary phytoplankton and nitrogen fixers become almost extinct in the S box because of severe nutrient limitation.

In the QM configuration, ordinary phytoplankton and nitrogen fixers persist in box S (grey bars in Fig. 2). The quadratic mortality reduces mortality at low phytoplankton concentrations and thereby prevents extinction of ordinary phytoplankton in the open ocean. Still, the main problems remain, i.e., nitrate vanishes in the UM box, the D box becomes anoxic, and more than 90 % of the initial $NO_3^-$ is lost.

In the RD configuration, complete $NO_3^-$ exhaustion in the UM box is prevented (bars with horizontal lines in Fig. 2). There is some observational evidence for the efficiency of decomposition of organic matter driven by denitrification in some high-productivity areas being lower than for respiratory processes in the presence of sufficient dissolved oxygen (Liu and Kaplan, 1984; Van Mooy et al., 2002). In our model, this mechanism helps preventing $NO_3^-$ depletion in the OMZ because less nitrate is consumed by denitrification during the passage of the particles through the OMZ. However, the additional organic matter now passing through the OMZ must be remineralized in the D box, which still becomes anoxic in this configuration.

The VD configuration, which supplies additional $O_2$ from the subtropical ocean into the D box, avoids anoxic deep waters, but fails to prevent nitrate exhaustion in the UM box (Fig. 8). The I and D boxes are oxic at steady state, but $NO_3^-$ is still exhausted by denitrification in the UM box. Comparing the oxygen concentrations of the RD configuration and VD configuration, we conclude that ventilation helps to prevent oxygen depletion in the D box, but this mechanism alone cannot prevent eventual run-away denitrification in the UM box. After incorporating reduced denitrification rate in the VDRD configuration, nitrate depletion is prevented and the I and D boxes are oxic (bars with vertical lines in Fig. 2). But the $O_2$ concentration in the I box is about 28 % lower than

that of the WOA2009 data, which indicates that $O_2$ supply into the D-box only may not be enough to ventilate the model domain.

The VID configuration, in which $O_2$ ventilation into the I box is also incorporated in addition to the D box, fails in preventing $NO_3^-$ depletion by denitrification in the OMZ (Fig. 8). Several sensitivity experiments were performed to explore how $NO_3^-$ depletion in the UM box can be prevented in the VID configuration. Decreasing the fraction for export production remineralized in the UM box ($f_{UM}$) from 70 % to 56 % makes $NO_3^-$ persist in the UM box. Together with the 20 % remineralization in the U box, this implies that 76 % of the export production is remineralized in the upper 500 m of the ocean. However, the $NO_3^-$ concentration in the UM box is only 3.8 $\mu$mol kg$^{-1}$, far away from the literature range from about 15 to 40 $\mu$mol L$^{-1}$. Next, a model of nitrogen fixation with an inverse relationship between $NO_3^-$ concentration and the fraction of fixed nitrogen from nitrogen fixation (Holl and Montoya, 2005; Mills and Arrigo, 2010) was implemented. This approach inhibits nitrogen fixation in an environment with high $NO_3^-$ concentrations, but fails to prevent $NO_3^-$ depletion in the UM box.

After reducing the denitrification rate in the OMZ, which is the configuration denoted as VIDRD, $NO_3^-$ depletion is prevented (bars with oblique lines in Fig. 2). Compared with the VDRD configuration, $O_2$ concentrations in the I box increase by about 21 %, closer to the WOA2009 data, however, $O_2$ concentration in the D box decreases due to a higher upwelling rate $A + B$ and slightly lower $O_2$ ventilation rate $K_H$ (Table 4).

In the OB configuration, nutrients are exchanged in addition to $O_2$ between the subtropical ocean and the I and D boxes. In this configuration, nitrate exhaustion in the OMZ is still not prevented even though there are lower phytoplankton and nitrogen fixer concentrations in the surface U and S boxes (Fig. 8). Again, after reducing the denitrification rate under suboxic conditions in the OBRD configuration, $N_{UM}$ depletion is prevented and $N_{UM}$ approaches a concentration of 20 $\mu$mol kg$^{-1}$ at steady state (bars with dots in Fig. 2). The UM box is suboxic and the $O_2$ concentrations in the I and D boxes agree very well with the WOA2009 data (gridded bars in Fig. 2). Overall, tracer

distributions simulated by the OBRD configuration agree best with the observations compared with other configurations.

## 3.2 Biogeochemical fluxes

For the biogeochemical fluxes, we will focus on the model configurations in Fig. 3, since they represent the most important mechanisms in preventing $NO_3^-$ exhaustion in the OMZ. The STD and QM configurations display very similar biogeochemical fluxes because the physical parameters in the two configurations are the same (black and grey bars in Fig. 3 respectively). However, denitrification rates are higher in the STD and QM configurations than in the RD configuration (bars with horizontal lines in Fig. 3), even though the physical parameters are the same in all three configurations, leading to nitrate exhaustion in the UM box of the STD and QM configurations but not in the RD configuration. In the VDRD configuration, $NO_3$ depletion is prevented (bars with vertical lines in panel E of Fig. 2). Compared with the VDRD configuration, the VIDRD configuration has a slightly higher denitrification rate and aerobic respiration rate in the OMZ because the altered transport parameters allow for a somewhat higher export production into the OMZ. Denitrification is weaker in the OBRD configuration than in the VIDRD configuration (bars with oblique lines in Fig. 3), even though the physical parameters are the same in both configurations, keeping more $NO_3^-$ in the UM-box in the OBRD configuration (bars with dots in Fig. 3). Aerobic respiration in the UM box continues even when the UM box is anoxic. It consumes all $O_2$ entering the UM box via the various physical transport processes and thereby oxidizes respectively about 9.9 %, 8.7 %, 64 %, 87 %, 85 % and 92 % of the organic matter remineralized (denitrification+ aerobic respiration) in the UM box in all six configurations. Aerobic respiration is increased in the OBRD configuration compared with the VIDRD configuration (92 % vs. 85 %) at the expense of denitrification.

Compared with the VIDRD configuration, total $PO_4^{3-}$ in the model domain decreases by about 28 % in the OBRD configuration at steady state, and the net $PO_4^{3-}$ flux out

**What prevents nitrogen depletion in the OMZ of the Eastern Tropical South Pacific?**

B. Su et al.

Title Page

| Abstract | Introduction |
| Conclusions | References |
| Tables | Figures |

◄◄ ►►

◄ ►

Back Close

Full Screen / Esc

Printer-friendly Version

Interactive Discussion

of the I box and the corresponding net flux of $PO_4^{3-}$ from the subtropical ocean into the D box causes a 9.6 % decrease in organic matter exported into the UM box. This explains why $NO_3^-$ concentrations in the OMZ and $O_2$ concentrations in the I and D boxes are slightly higher (bars with oblique lines and bars with dots in Fig. 2). Re-
5 stricting exchange with the subtropical oligotrophic ocean to $NO_3^-$ and $O_2$ cannot result in higher $O_2$ concentrations in the I and D boxes, because it does not reduce the export production to be decomposed there. Restricting exchange to $PO_4^{3-}$ and $O_2$ de-presses production and organic matter decomposition by almost the same amount as in the model run that exchanges $NO_3^-$, $PO_4^{3-}$ and $O_2$, and succeeds in driving $O_{2I}$ and
10 $O_{2D}$ concentrations closer to the observations (not shown). Thus, opening the model boundary to $PO_4^{3-}$ and $O_2$ helps to improve the behaviour of VIDRD configuration by depressing biological production in the upwelling region.

The fluxes associated with the fixed-N cycle in the OMZ of the OB configuration are compared with those of other models in Table 6. Our simulated export production
15 and aerobic remineralization are mostly consistent with the results of Kalvelage et al. (2013), but our simulated anaerobic remineralization and fixed-N loss in the OMZ are much lower. However, our model's fixed-N loss due to denitrification is between the values reported by Mills and Arrigo (2010) and Kalvelage et al. (2013). The Kalvelage et al. (2013) model has much higher fixed-N influx into the OMZ via physical transport,
20 which could compensate for their more intense $NO_3^-$ loss in the OMZ.

In sensitivity experiments designed to elucidate the importance of the influence of the subtropical ocean on the model domain, we reduce the mixing rates ($K_H$) of $O_2$, $NO_3^-$ and $PO_4^{3-}$ across the southern boundary in different combinations (Fig. 4). Total net primary production (NPP) is the same when varying the mixing rate of either only
25 $O_2$ or $O_2$ together with $NO_3^-$, as long as the $PO_4^{3-}$ exchange rate with the subtropical ocean remains unchanged (dotted lines in Fig. 4b and g). The reason is that changes in nitrate exchange with the subtropical ocean are compensated by changes in den-itrification and nitrogen fixation.This implies that NPP is, at steady state, determined only by phosphate availability. Once the total NPP of NF and Phy is determined by

What prevents nitrogen depletion in the OMZ of the Eastern Tropical South Pacific?

B. Su et al.

Full Screen / Esc

Printer-friendly Version

Interactive Discussion

Printer-friendly Version

Interactive Discussion

$PO_4^{3-}$ supply, aerobic respiration will increase with increasing $O_2$ supply, while anaerobic remineralization will decrease (solid lines in Fig. 4c and h). Comparing simulations that vary the mixing rate of $O_2$ together with that of $PO_4^{3-}$, with simulations that vary the mixing rate of $O_2$ together with that of $NO_3^-$ and $PO_4^{3-}$ (dotted lines in Fig. 4l and q)

5 reveals that the combined NPP of Phy and NF decreases with decreasing $PO_4^{3-}$ inventory at low mixing rates and increases with increasing $PO_4^{3-}$ inventory at hight mixing rates, irrespective of $NO_3^-$ mixing rate.

It turns out that $NO_3^-$ depletion in the OMZ is prevented in the four sensitivity experiments of Fig. 4 no matter how much $O_2$ is supplied from the subtropical ocean into the

10 model domain. But anoxia in the D box can only be prevented if the external $O_2$ supply can oxidise more than about 20 % export production in the model domain (solid lines in Fig. 4e, j, o and t). These experiments also reveal an interesting link among the $O_2$ supply from the subtropical ocean, the nitrate concentration in the OMZ, and the $NO_3^-$ flux between the model domain and surrounding ocean. As soon as the $O_2$ supply from

15 the subtropical ocean accounts for about 17.5 % of the respiratory $O_2$ consumption, the model domain turns into a small net source of fixed-N (dashed lines in the first row of Fig. 4). Once anoxia is prevented in the D box, the nitrate concentration in the OMZ (UM box) increases quite strongly from about 15 $\mu mol\,kg^{-1}$ to reach about 20 $\mu mol\,kg^{-1}$ at full mixing strength.

20 The behaviour of the model domain as a small pelagic net $NO_3^-$ source in the OBRD configuration is rather insensitive to the physical transport parameters (Fig. 5). The model domain remains a net $NO_3^-$ source even when the physical transport parameters are varied by up to ±50 %. The finding that the model domain is a net $NO_3^-$ source is also tenable for all suites of physical transport parameters in the literature range for

25 which the D-box is oxic (Fig. 7).

The oxygen concentrations in the UM, I and D boxes increase in sensitivity model runs with physical parameters calibrated from increased ^{14}C concentrations (lower water mass age). $NO_3^-$ depletion is prevented in the OMZ in the OBRD configuration within

the range of about $\pm 10\%$ around the default ventilation intensity (Fig. 6a). The UM box remains anoxic when $\Delta^{14}C$ is varied within this range, which indicates that this mechanism for preventing $NO_3^-$ depletion in the OMZ may be robust against modest changes in the regional ocean circulation patterns. Meanwhile, $NO_3^-$ and $O_2$ in the UM box are quite insensitive to the $O_2$ concentration in the U-box for this configuration (Fig. 6b).

## 4   Discussion and conclusions

Nitrogen is often considered to be the primary limiting nutrient in marine upwelling regions with OMZs (Cline and Richards, 1972; Codispoti and Christensen, 1985; Morrison et al., 1998; Voss et al., 2001), where denitrification rates can be high and are generally thought to cause a major loss of fixed-N from the world ocean. The nitrogen deficit is commonly assumed to stimulate $N_2$ fixation, both in observational estimates of $N_2$ fixation (Deutsch et al., 2007; Monteiro et al., 2010) and in current descriptions of $N_2$ fixation in biogeochemical models (Moore and Doney, 2007; Schmittner et al., 2008). However, if $N_2$ fixation is tightly linked to nitrogen loss processes, denitrification of organic matter derived from $N_2$ fixation can consume more nitrogen than was fixed via $N_2$ fixation and thereby lead to a vicious cycle of run-away nitrogen loss (Landolfi et al., 2013). This has been found to lead to total depletion of $NO_3^-$ in the OMZ of box models (Canfield, 2006) and global biogeochemical circulation models (Moore and Doney, 2007; Schmittner et al., 2008). For our fully prognostic 5-box model, we have identified the mechanisms capable of arresting the run-away nitrogen loss that can result from a close coupling of nitrogen fixation and denitrification (Landolfi et al., 2013) and maintaining realistic non-zero $NO_3^-$ concentrations in open-ocean OMZs of the ETSP: reduced $NO_3^-$ consumption by denitrification owing to slower remineralization under suboxic compared to oxic conditions, coupled with lateral ventilation between the model domain and an ocean basin outside of the model domain (the subtropical ocean in this case).

**What prevents nitrogen depletion in the OMZ of the Eastern Tropical South Pacific?**

B. Su et al.

In this work, the model configuration with reduced denitrification rate and lateral ventilation and nutrient exchange (OBRD configuration) behaves most reasonable, whereas reduced rates of denitrification alone leads to unrealistic $O_2$ depletion in the deep waters, and reduced rates of denitrification combined with only $O_2$ ventilation in the D or both I and D boxes configurations do worse in fitting the WOA2009 data for $O_2$ in the I and D boxes. By allowing for exchange of $O_2$ and nutrients with the subtropical ocean in the OBRD configuration, the delicate balance between sufficient $O_2$ supply required for maintaining high levels of aerobic respiration and sufficient $PO_4^{3-}$ loss through the open boundary appears fulfilled. Compared with other box models (Shaffer and Sarmiento, 1995; Tyrrell, 1999; Deutsch et al., 2004; Canfield, 2006; Mills and Arrigo, 2010; Eugster and Gruber, 2012; DeVries et al., 2012), the box model we use here explicitly employs both a reduced-denitrification rate and an open boundary condition, which seems to be a prerequisite for the ability to simulate realistic nitrate conditions in the OMZ and oxygen concentrations in the adjacent ocean.

Phosphate turns out as the ultimate limiting nutrient in our model (second and forth rows of Fig. 4), and hence determines the nitrogen content of the OMZ. This strong control of phosphate on the N cycle is similar to the finding of previous studies (e.g. Lenton and Watson, 2000; Canfield, 2006), where the occurrence and extent of oceanic anoxia was also tightly linked to phosphate supply. These studies explicitly assumed that $N_2$ fixation acts to restore surface-oceanic dissolved inorganic N : P ratio towards the Redfield ratio. By contrast, we do not prescribe the effect of nitrogen fixation on surface inorganic nutrients, and the finding of phosphate as the ultimate limiting nutrient is obtained regardless of whether NF responds directly to the N : P ratio in the surface ocean or whether NF is inhibited by the presence of $NO_3^-$ (see Appendix D).

Even though our model indicates only a weak dependence of simulated $NO_3^-$ concentrations in the OMZ on the lateral $O_2$ supply from the subtropical ocean, $O_2$ depletion in the adjacent ocean can be prevented only when the $O_2$ supply from the subtropical ocean accounts for more than 20 % of the $O_2$ required to oxidize export production from the surface ocean of our model domain (U and S boxes). This value only varies

from about 17 % to 23 %, when the size of the S box varies by ±50 %, indicating that our above conclusion is insensitive to our choice for the model domain. The $O_2$ supply from the subtropical ocean might be also linked to the balance of the regional fixed-N cycle. In the most realistic (OBRD) configuration, the balance of water-column denitrification and nitrogen fixation is tightly linked to the nitrate concentration in the OMZ: if the model domain acts as a sink for fixed-N, nitrate concentrations in the OMZ do not exceed about 15 µmol kg$^{-1}$, i.e., the lower limit of current observations, 15 to 40 µmol kg$^{-1}$ (Codispoti and Richards, 1976; Codispoti and Packard, 1980; Morrison et al., 1998; Voss et al., 2001). Nitrate concentrations close to those commonly found in OMZs are predicted only when nitrogen fixation exceeds water-column denitrification and the ocean basin containing the OMZ becomes a net source of fixed-N (first row of Fig. 4).

There are no specific data or model results focusing on the water-column nitrogen balance of the ETSP. Our simulations using a parameterisation where nitrogen fixation is inhibited by the presence of nitrate yield very similar results, only with slightly reduced nitrogen fixation resulting in a somewhat reduced (by ≤ 15 %) nitrogen source for strong enough lateral oxygen supply. Ganachaud and Wunsch (2002) estimated a net northward $NO_3$ transport of 270 ± 170 kmol s$^{-1}$ (119.2 ± 75.1 Tg N yr$^{-1}$) across 17° S into the ETSP indicating that the ETSP is a net nitrogen sink, but their estimate included benthic denitrification, which is not accounted for in our current analysis. In a model-guided analysis, DeVries et al. (2012) predicted water-column denitrification rates of 21–33 Tg N yr$^{-1}$ by simulating the distribution of observed dissolved $N_2$ gas produced by denitrifying bacteria. From an analysis of nutrient concentrations and transport rates, Deutsch et al. (2007) estimated nitrogen fixation rates in the Pacific Ocean of about 95 Tg N yr$^{-1}$, half of which was speculated to occur in the ETSP. From these estimates, we cannot rule out that the water column of the ETSP is a net source of fixed-N, which would be consistent with our results obtained in the OBRD configuration. More recently, Eugster and Gruber (2012) probabilistically estimated nitrogen fixation and water-column and benthic denitrification separately, and we find that the

water column of the IndoPacific is a large fixed-N source when we estimated the fixed-N budget for that regions, which appears to be consistent with our results.

Based on our model results, we conclude that reduced $NO_3^-$ consumption by denitrification owing to slower remineralization under suboxic conditions together with lateral transport is essential to arrest the vicious cycle of run-away fixed-N loss in the OMZ. More research is needed to better constrain the model parameters, in particular the upwelling transport and the difference between the organic matter remineralisation rate via aerobic respiration and anaerobic denitrification.

## Appendix A:

Physical transports of a tracer $X$ among the boxes U, UM, S, I, and D are defined for the STD configuration as follows:

$$\text{Transport}(X_U) = (X_{UM} - X_U)(A + B + K_{US}) \cdot L_U \tag{A1}$$

$$\text{Transport}(X_{UM}) = \left[ AX_D + BX_I - X_{UM}(A + B) + K_{US}(X_U - X_{UM}) \right] \cdot L_U$$
$$+ K_{UM}(X_D - X_{UM}) \cdot L_U + K_H(X_I - X_{UM}) \cdot H_{UM} \tag{A2}$$

$$\text{Transport}(X_S) = (A + B)(X_U - X_S) \cdot L_U + K_{US}(X_I - X_S) \cdot L_S \tag{A3}$$

$$\text{Transport}(X_I) = (A + B)(X_S - X_I) \cdot L_U + K_H(X_{UM} - X_I) \cdot H_{UM}$$
$$+ K_{US}(X_S - X_I) \cdot L_S + K_{UM}(X_D - X_I) \cdot L_S \tag{A4}$$

$$\text{Transport}(X_D) = A (X_I - X_D) \cdot L_U + K_{UM}(X_{UM} - X_D) \cdot L_U + K_{UM}(X_I - X_D) \cdot L_S \tag{A5}$$

For the VD, VDRD, VID, VIDRD, OB and OBRD configurations, Eqs. (A4) and (A5) are modified to read:

$$\text{Transport}(X_I) = (A + B)(X_S - X_I) \cdot L_U + K_H(X_{UM} - X_I) \cdot H_{UM}$$
$$+ K_{US}(X_S - X_I) \cdot L_S + K_{UM}(X_D - X_I) \cdot L_S$$
$$+ K_H(X_{SI} - X_I) \cdot H_{UM} \tag{A6}$$

$$\text{Transport}(X_D) = A (X_I - X_D) \cdot L_U + K_{UM}(X_{UM} - X_D) \cdot L_U + K_{UM}(X_I - X_D) \cdot L_S$$
$$+ K_H(X_{SD} - X_D) \cdot H_D \tag{A7}$$

The transport equations (Eqs. A1 and A3) are modified for Phy and NF because Phy and NF are assumed to be capable of regulating their buoyancy and exist only in U and S without being transported vertically between the U and UM or the S and I boxes.

## Appendix B:

The nitrogen cycle in this model includes nitrogen fixation, denitrification, inorganic nitrogen regeneration by remineralization, and physical transport of nitrogen. The physical transport process of $NO_3^-$ is the same as for other tracers. $\text{Rem}_i^N$ represents nitrogen remineralization in box $i$ with fixed fractions $f_i$ of the net primary production in the overlaying surface boxes.

$$\text{Rem}_U^N = f_U M(\text{Phy}_U + \text{NF}_U) \cdot H_U \cdot L_U \tag{B1}$$
$$\text{Rem}_{UM}^N = f_{UM} M(\text{Phy}_U + \text{NF}_U) \cdot H_U \cdot L_U \tag{B2}$$
$$\text{Rem}_S^N = f_S M(\text{Phy}_S + \text{NF}_S) \cdot H_U \cdot L_S \tag{B3}$$
$$\text{Rem}_I^N = f_I M(\text{Phy}_S + \text{NF}_S) \cdot H_U \cdot L_S \tag{B4}$$
$$\text{Rem}_D^N = M \big[ (1 - f_U - f_{UM})(\text{Phy}_U + \text{NF}_U) \cdot L_U$$
$$+ (1 - f_S - f_I)(\text{Phy}_S + \text{NF}_S) \cdot L_S \big] \cdot H_U \tag{B5}$$

Denitrification (Denif) is the nitrogen loss to $N_2$ when UM, I and D are anoxic. It is defined as:

$$\text{Denif}_i = \max(\text{Rem}_i^N - \frac{\text{Res}_i}{r_a}, 0) \cdot \frac{r_c}{r_{den}} \quad i \in [\text{UM, I, D}] \tag{B6}$$

with the aerobic respiration term Res$_i$ given below (Eq. B10). In the RD, VDRD, VIDRD and OBRD configuration, the equations for denitrification in the *i* box and remineralization in D are given by:

$$\text{Denif}_i = \frac{1}{5} \cdot \max\left(\text{Rem}_i^N - \frac{\text{Res}_i}{r_a}, 0\right) \cdot \frac{r_c}{r_{den}} \quad i \in [\text{UM, I}] \tag{B7}$$

$$\text{Rem}_D^N = M\left[(1 - f_U - f_{UM})(\text{Phy}_U + \text{NF}_U) \cdot L_U + (1 - f_S - f_I)(\text{Phy}_S + \text{NF}_S) \cdot L_S\right] \cdot H_U$$

$$+ 4 \cdot \frac{\text{Denif}_i \cdot r_{den}}{r_c} \quad i \in [\text{UM, I}] \tag{B8}$$

All the organic matter is composed according to the Redfield Ratio, i.e., C : N : P = 106 : 16 : 1. $\text{Rem}_i^P$ represents phosphate remineralization in box *i*, which is obtained by dividing $\text{Rem}_i^N$ by the Redfield N : P ratio, $r_p$:

$$\text{Rem}_i^P = \frac{\text{Rem}_i^N}{r_p} \quad i \in [\text{U, S, UM, I, D}] \tag{B9}$$

Respiration (Res$_i$) is considered in the intermediate and deep ocean. In the presence of sufficient oxygen or when oceanic circulation supplies enough O$_2$, organic matter will be preferentially oxidized by respiration. We use a ratio of $-\text{O}_2 : \text{N} = 170 : 16$ during oxic remineralization of organic matter (Anderson and Sarmiento, 1994).

$$\text{Res}_i = \begin{cases} r_a \cdot \text{Rem}_i^N & \text{if } \text{O}_{2i} > 0 \\ \min\left(\text{Transport}(\text{O}_{2i}), r_a \cdot \text{Rem}_i^N\right) & \text{if } \text{O}_{2i} = 0 \end{cases} \quad i \in [\text{UM, I, D}] \tag{B10}$$

## Appendix C:

Transport and SMS terms for $\widehat{^{14}\text{C}}$ constitute a system of 5 linear equations including transport parameters $A$, $B$, $K_{US}$, $K_{UM}$ and $K_H$, which are inverted from the $\Delta^{14}$C values with air–sea $\Delta^{14}$C exchange rates $g_U$ and $g_S$ for the U and S boxes respectively.

$g_U$ and $g_S$ were constrained in a two-step procedure. First, all combinations are determined which result in transport parameters in the literature range in Table 5. Finally, the combination giving the most realistic biogeochemical tracer concentrations (closest to observations) is chosen for the experiments in the main text (Fig. 8). This approach for determining the physical transport parameters is applied to obtain the ones in Table 4.

**Appendix D:**

It is well known from laboratory studies that diazotrophic phytoplankton can also utilize nitrate for growth (e.g., Holl and Montoya, 2005). Schmittner et al. (2008) introduced a formulation where nitrogen fixers preferentially use nitrate when available and cover only the residual nitrogen demand via $N_2$ fixation. In order to examine the behavior of our model when nitrogen fixers (NF) preferentially use nitrate, nitrogen fixation is separated from diazotroph growth, as in Schmittner et al. (2008):

$$\text{Nitrogen-fixation}_i = \left(1 - \frac{N}{N + N_h}\right) \cdot \text{NPP}^{\text{NF}_i} \qquad i \in [U, S] \tag{D1}$$

and Eq. (6) was modified to accomodate the additional nitrate uptake by NF as follows:

$$\text{SMS}(N_i) = \left(-\text{NPP}^{\text{Phy}_i} - \left(\text{NPP}^{\text{NF}_i} - \text{Nitrogen-fixation}_i\right)\right) \cdot V_i + \text{Rem}_i^N - \text{Denif}_i$$
$$i \in [U, UM, S, I, D] \tag{D2}$$

Model results for all configurations with Eqs. (D1) and (D2) are presented in Fig. 9. Compared to Fig. 2, this configuration behaves very similarly, except that $\text{Phy}_U$ and $\text{Phy}_S$ concentrations are somewhat lower because nitrogen fixers take up $NO_3^-$ as well. Thus, we conclude that our results are robust with respect to assumptions about fixed-N usage by diazotrophs.

## References

Anderson, L. A. and Sarmiento, J. L.: Redfield ratios of remineralization determined by nutrient data analysis, Global Biogeochem. Cy., 8, 65–80, doi:10.1029/93GB03318, 1994. 11116

Bethoux, J. P.: Oxygen consumption, new production, vertical advection and environmental evolution in the Mediterranean Sea, Deep-Sea Res., 36, 769–781, doi:10.1016/0198-0149(89)90150-7, 1989. 11097

Bulow, S. E., Rich, J. J., Naik, H. S., Pratihary, A. K., and Ward, B. B.: Denitrification exceeds anammox as a nitrogen loss pathway in the Arabian Sea oxygen minimum zone, Deep-Sea Res. Pt. I, 57, 384–393, doi:10.1016/j.dsr.2009.10.014, 2010. 11099

Canfield, D.: Models of oxic respiration, denitrification and sulfate reduction in zones of coastal upwelling, Geochim. Cosmochim. Ac., 70, 5753–5765, doi:10.1016/j.gca.2006.07.023, 2006. 11097, 11111, 11112, 11128

Capone, D. G. and Knapp, A. N.: A marine nitrogen cycle fix?, Nature, 445, 159–160, doi:10.1038/445159a, 2007. 11097

Capone, D. G., Zehr, J. P., Paerl, H. W., Bergman, B., and Carpenter, E. J.: *Trichodesmium*, a globally significant marine cyanobacterium, Science, 276, 1221–1229, doi:10.1126/science.276.5316.1221, 1997. 11128

Caron, D. A. and Dennett, M. R.: Phytoplankton growth and mortality during the 1995 Northeast Monsoon and Spring Intermonsoon in the Arabian Sea, Deep-Sea Res. Pt. II, 46, 1665–1690, doi:10.1016/S0967-0645(99)00039-9, 1999. 11128

Cline, J. D. and Richards, F. A.: Oxygen deficient conditions and nitrate reduction in the Eastern Tropical North Pacific Ocean, Limnol. Oceanogr., 17, 885–900, 1972. 11111

Title Page

Abstract | Introduction

Conclusions | References

Tables | Figures

◄◄ | ►►

◄ | ►

Back | Close

Full Screen / Esc

Printer-friendly Version

Interactive Discussion

Codispoti, L. A.: Is the ocean losing nitrate?, Nature, 376, 724, doi:10.1038/376724a0, 1995. 11099

Codispoti, L. A.: An oceanic fixed nitrogen sink exceeding 400 Tg N a$^{-1}$ vs the concept of homeostasis in the fixed-nitrogen inventory, Biogeosciences, 4, 233–253, doi:10.5194/bg-4-233-2007, 2007. 11097

Codispoti, L. A. and Christensen, J.: Nitrification, denitrification and nitrous oxide cycling in the Eastern Tropical South Pacific Ocean, Mar. Chem., 16, 277–300, doi:10.1016/0304-4203(85)90051-9, 1985. 11111

Codispoti, L. A. and Packard, T.: Denitrification rates in the eastern tropical South Pacific, J. Mar. Res., 38, 453–477, 1980. 11097, 11113

Codispoti, L. A. and Richards, F.: An analysis of the horizontal regime of denitrification in the eastern tropical North Pacific, Limnol. Oceanogr., 21, 379–388, 1976. 11097, 11113

Codispoti, L. A., Brandes, J., Christensen, J., Devol, A., Naqvi, S., Paerl, H., and Yoshinari, T.: The oceanic fixed nitrogen and nitrous oxide budgets: moving targets as we enter the anthropocene?, Sci. Mar., 65, doi:10.3989/scimar.2001.65s285, 2001. 11097

Dalsgaard, T., Thamdrup, B., and Canfield, D. E.: Anaerobic ammonium oxidation (anammox) in the marine environment, Res. Microbiol., 156, 457–464, doi:10.1016/j.resmic.2005.01.011, 2005. 11097

Deutsch, C., Sigman, D. M., Thunell, R. C., Meckler, A. N., and Haug, G. H.: Isotopic constraints on glacial/interglacial changes in the oceanic nitrogen budget, Global Biogeochem. Cy., 18, doi:10.1029/2003GB002189, 2004. 11112

Deutsch, C., Sarmiento, J. L., Sigman, D. M., Gruber, N., and Dunne, J. P. Spatial coupling of nitrogen inputs and losses in the ocean, Nature, 445, 163–167, doi:10.1038/nature05392, 2007. 11098, 11111, 11113

DeVries, T., Deutsch, C., Primeau, F., Chang, B., and Devol, A.: Global rates of water-column denitrification derived from nitrogen gas measurements, Nature, 5, 547–550, doi:10.1038/NGEO1515, 2012. 11112, 11113

Eppley, R. W., Rogers, J. N., and McCarthy, J. J.: Half-saturation constants for uptake of nitrate and ammonium by marine phytoplankton, Limnol. Oceanogr., 14, 912–920, doi:10.4319/lo.1969.14.6.0912, 1969. 11128

Eugster, O. and Gruber, N.: A probabilistic estimate of global marine N-fixation and denitrification, Global Biogeochem. Cy., 26, 1–15, doi:10.1029/2012GB004300, 2012. 11097, 11112, 11113

**What prevents nitrogen depletion in the OMZ of the Eastern Tropical South Pacific?**

B. Su et al.

Title Page

| Abstract | Introduction |
| Conclusions | References |
| Tables | Figures |

◀ | ▶

◀ | ▶

Back | Close

Full Screen / Esc

Printer-friendly Version

Interactive Discussion

Fernandez, C., Farías, L., and Ulloa, O.: Nitrogen fixation in denitrified marine waters, PLoS ONE, 6, e20539, doi:10.1371/journal.pone.0020539, 2011. 11098

Furnas, M. J.: In situ growth rates of marine phytoplankton: approaches to measurement, community and species growth rates, J. Plankton Res., 12, 1117–1151, doi:10.1093/plankt/12.6.1117, 1990. 11128

Galloway, J. N., Dentener, F. J., Capone, D. G., Boyer, E. W., Howarth, R. W., Seitzinger, S. P., Asner, G. P., Cleveland, C. C., Green, P. A., Holland, E. A., Karl, D. M., Michaels, A. F. Porter, J. H., Townsend, A. R., and Vörösmarty, C. J.: Nitrogen cycles: past, present and future, Biogeochemistry, 70, 153–226, doi:10.1007/s10533-004-0370-0, 2004. 11097

Ganachaud, A. and Wunsch, C.: Oceanic nutrients and oxygen transports and bounds on export production during the World Ocean Circulation Experiment, Global Biogeochem. Cy., 16, 1–14, doi:10.1029/2000GB001333, 2002. 11113

Garcia, H. E., Locarnini, R. A., Boyer, T. P., Antonov, J. I., Baranova, O. K., Zweng, M. M., and Johnson, D. R.: Volume 3: dissolved oxygen, apparent oxygen utilization, and oxygen saturation, in: World Ocean Atlas 2009, edited by: Levitus, S., NOAA Atlas NESDIS 70, US Government Printing Office, Washington, D. C., p. 344, 2010a. 11102

Garcia, H. E., Locarnini, R. A., Boyer, T. P., Antonov, J. I., Zweng, M. M., Baranova, O. K., and Johnson, D. R.: Volume 4: nutrients (phosphate, nitrate, silicate), in: World Ocean Atlas 2009, NOAA Atlas NESDIS 71, US Government Printing Office, Washington, D. C., p. 398, 2010b. 11102

Gruber, N.: The dynamics of the marine nitrogen cycle and its influence on atmospheric $CO_2$ variations, in: The Ocean Carbon Cycle and Climate, edited by: Follows, M. and Oguz, T., vol. 40 of NATO Science Series, Kluwer Academic, Dordrecht, the Netherlands, chap. 4, 97–148, 2004. 11097

Gruber, N. and Sarmiento, J. L.: Global patterns of marine nitrogen fixation and denitrification, Global Biogeochem. Cy., 11, 235–266, doi:10.1029/97GB00077, 1997. 11096, 11097

Hamersley, M. R., Lavik, G., Woebken, D., Rattray, J. E., Lam, P., Hopmans, E. C., Damsté, J. S. S., Krüger, S., Graco, M., Gutiérrez, D., and Kuypers, M. M. M.: Anaerobic ammonium oxidation in the Peruvian oxygen minimum zone, Limnol. Oceanogr., 52, 923–933, doi:10.4319/lo.2007.52.3.0923, 2007. 11099

Holl, C. M. and Montoya, J. P.: Interactions between nitrate uptake and nitrogen fixation in continuous cultures of the marine diazotroph *Trichodesmium* (cyanobacteria), J. Phycol., 41, 1178–1183, doi:10.1111/j.1529-8817.2005.00146.x, 2005. 11107, 11117

**What prevents nitrogen depletion in the OMZ of the Eastern Tropical South Pacific?**

B. Su et al.

Kalvelage, T., Lavik, G., Lam, P., Contreras, S., Arteaga, L., Löscher, C. R., Oschlies, A., Paulmier, A., Stramma, L., and Kuypers, M. M. M.: Nitrogen cycling driven by organic matter export in the South Pacific oxygen minimum zone, Nat. Geosci., 6, 228–234, doi:10.1038/NGEO1739, 2013. 11109, 11129

5  Key, R. M., Kozyr, A., Sabine, C. L., Lee, K., Wanninkhof, R., Bullister, J. L., Feely, R. A., Millero, F. J., Mordy, C., and Peng, T.-H.: A global ocean carbon climatology: results from Global Data Analysis Project (GLODAP), Global Biogeochem. Cy., 18, 1–23, doi:10.1029/2004GB002247, 2004. 11099, 11102

Kuypers, M. M. M., Lavik, G., Woebken, D., Schmid, M., Fuchs, B. M., Amann, R., Jørgensen, B. B., and Jetten, M. S. M.: Massive nitrogen loss from the Benguela upwelling system through anaerobic ammonium oxidation, P. Natl. Acad. Sci. USA, 102, 6478–6483, doi:10.1073/pnas.0502088102, 2005. 11099

La Roche, J. and Breitbarth, E.: Importance of the diazotrophs as a source of new nitrogen in the ocean, J. Sea Res., 53, 67–91, doi:10.1016/j.seares.2004.05.005, 2005. 11101

15  Landolfi, A., Dietze, H., Koeve, W., and Oschlies, A.: Overlooked runaway feedback in the marine nitrogen cycle: the vicious cycle, Biogeosciences, 10, 1351–1363, doi:10.5194/bg-10-1351-2013, 2013. 11097, 11111

Lenton, T. M. and Watson, A. J.: Redfield revisited 1. Regulation of nitrate, phosphate, and oxygen in the ocean, Global Biogeochem. Cy., 14, 225–248, doi:10.1029/1999GB900065, 2000. 11112

Libby, W. F.: Radiocarbon dating, Am. Sci., 44, 98–112, 1956. 11128

Liu, K.-K. and Kaplan, I. R.: Denitrification rates and availability of organic matter in marine environments, Earth Planet. Sc. Lett., 68, 88–100, doi:10.1016/0012-821X(84)90142-0, 1984. 11106

25  Martin, J. H., Knauer, G. A., Karl, D. M., and Broenkow, W. W.: VERTEX: carbon cycling in the northeast Pacific, Deep-Sea Res., 34, 267–285, 1987. 11128

McAllister, C. D., Shah, N., and Strickland, J. D. H.: Marine phytoplankton photosynthesis as a function of light intensity: a comparison of methods, J. Fish. Res. Board Can., 21, 159–181, doi:10.1139/f64-010, 1964. 11128

30  Mills, M. M. and Arrigo, K. R.: Magnitude of oceanic nitrogen fixation influenced by the nutrient uptake ratio of phytoplankton, Nat. Geosci., 3, 412–416, doi:10.1038/NGEO856, 2010. 11098, 11107, 11109, 11112, 11129

**What prevents nitrogen depletion in the OMZ of the Eastern Tropical South Pacific?**

B. Su et al.

Mills, M. M., Ridame, C., Davey, M., La Roche, J., and Geider, R. J.: Iron and phosphorus co-limit nitrogen fixation in the eastern tropical North Atlantic, Nature, 429, 292–232, doi:10.1038/nature02550, 2004. 11101

Molina, V. and Farías, L.: Aerobic ammonium oxidation in the oxycline and oxygen minimum zone of the eastern tropical South Pacific off northern Chile ($\sim 20^\circ$ S), Deep-Sea Res. Pt. II, 56, 1032–1041, doi:10.1016/j.dsr2.2008.09.006, 2009. 11099

Monteiro, F. M., Follows, M. J., and Dutkiewicz, S.: Distribution of diverse nitrogen fixers in the global ocean, Global Biogeochem. Cy., 24, 1–16, doi:10.1029/2009GB003731, 2010. 11111

Moore, J. K. and Doney, S. C.: Iron availability limits the ocean nitrogen inventory stabilizing feedbacks between marine denitrification and nitrogen fixation, Global Biogeochem. Cy., 21, 1–12, doi:10.1029/2006GB002762, 2007. 11098, 11111

Morrison, J., Codispoti, L., Gaurin, S., Jones, B., Manghnani, V., and Zheng, Z.: Seasonal variation of hydrographic and nutrient fields during the US JGOFS Arabian Sea Process Study, Deep-Sea Res. Pt. II, 45, 2053–2101, doi:10.1016/S0967-0645(98)00063-0, 1998. 11097, 11111, 11113

Palmer, J. and Totterdell, I.: Production and export in a global ocean ecosystem model, Deep-Sea Res. Pt. I, 48, 1169–1198, doi:10.1016/S0967-0637(00)00080-7, 2001. 11128

Paulmier, A. and Ruiz-Pino, D.: Oxygen minimum zones (OMZs) in the modern ocean, Prog. Oceanogr., 80, 113–128, doi:10.1016/j.pocean.2008.08.001, 2009. 11097

Redfield, A. C., Ketchum, B. H., and Richards, F. A.: The influence of organisms on the composition of sea-water, in: The Sea, 26–77, 1963. 11101

Robarts, R. D. and Zohary, T.: Temperature effects on photosynthetic capacity, respiration, and growth rates of bloom forming cyanobacteria, New Zeal. J. Mar. Fresh., 21, 391–399, doi:10.1080/00288330.1987.9516235, 1987. 11128

Schmittner, A., Oschlies, A., Matthews, H. D., and Galbraith, E. D.: Future changes in climate, ocean circulation, ecosystems, and biogeochemical cycling simulated for a business-as-usual $CO_2$ emission scenario until year 4000 AD, Global Biogeochem. Cy., 21, doi:10.1029/2007GB002953, 2008. 11098, 11104, 11111, 11117, 11128

Shaffer, G. and Sarmiento, J. L.: Biogeochemical cycling in the global ocean 1. A new, analytical model with continuous vertical resolution and high-latitude dynamics, J. Geophys. Res., 100, 2659–2672, doi:10.1029/94JC01167, 1995. 11102, 11112

Suess, E.: Particulate organic carbon flux in the ocean surface productivity and oxygen utilization, Nature, 288, 260–263, doi:10.1038/288260a0, 1980. 11128

**What prevents nitrogen depletion in the OMZ of the Eastern Tropical South Pacific?**

B. Su et al.

Toggweiler, J. R., Dixon, K., and Bryan, K.: Simulations of radiocarbon in a coarse-resolution world ocean model 1. Steady state prebomb distributions, J. Geophys. Res., 94, 8217–8242, doi:10.1029/JC094iC06p08217, 1989. 11102

Tyrrell, T.: The relative influences of nitrogen and phosphorus on oceanic primary production, Nature, 400, 525–531, 1999. 11112

Van Mooy, B. A. S., Keil, R. G., and Devol, A. H.: Impact of suboxia on sinking particulate organic carbon: enhanced carbon flux and preferential degradation of amino acids via denitrification, Geochim. Cosmochim. Ac., 66, 457–467, doi:10.1016/S0016-7037(01)00787-6, 2002. 11106

Voss, M., Dippner, J. W., and Montoya, J. P.: Nitrogen isotope patterns in the oxygen-deficient waters of the Eastern Tropical North Pacidic Ocean, Deep-Sea Res. Pt. I, 48, 1905–1921, doi:10.1016/S0967-0637(00)00110-2, 2001. 11097, 11111, 11113

Ward, B. B., Devol, A. H., Rich, J. J., Chang, B. X., Bulow, S. E., Naik, H., Pratihary, A., and Jayakumar, A.: Denitrification as the dominant nitrogen loss process in the Arabian Sea, Nature, 461, 78–81, doi:10.1038/nature08276, 2009. 11099

**What prevents nitrogen depletion in the OMZ of the Eastern Tropical South Pacific?**

B. Su et al.

Title Page

| Abstract | Introduction |
| Conclusions | References |
| Tables | Figures |

◄◄  ►►

◄  ►

Back  Close

Full Screen / Esc

Printer-friendly Version

Interactive Discussion

**Table 1.** Model variables.

| Variables | Units | Description | Equation |
|-----------|-------|-------------|----------|
| $Phy_i$ | $\mu mol\,N\,kg^{-1}$ | Ordinary phytoplankton in box $i$ | Eq. (2) |
| $NF_i$ | $\mu mol\,N\,kg^{-1}$ | Nitrogen fixers in box $i$ | Eq. (3) |
| $N_i$ | $\mu mol\,N\,kg^{-1}$ | Nitrate concentration in box $i$ | Eq. (6) |
| $N_{avg}$ | $\mu mol\,N\,kg^{-1}$ | Average nitrogen concentration | [a] |
| $P_i$ | $\mu mol\,P\,kg^{-1}$ | Phosphate concentration in box $i$ | Eq. (7) |
| $P_{avg}$ | $\mu mol\,P\,kg^{-1}$ | Average phosphorus concentration | [b] |
| $O_{2i}$ | $\mu mol\,kg^{-1}$ | Oxygen concentration in box $i$ | Eq. (8) |

[a] $N_{avg} = \dfrac{(N_U+Phy_U+NF_U)\cdot V_U+N_{UM}\cdot V_{UM}+(N_S+Phy_S+NF_S)\cdot V_S+N_I\cdot V_I+N_D\cdot V_D}{V_U+V_{UM}+V_S+V_I+V_D}$

[b] $P_{avg} = \dfrac{\left(P_U+\frac{Phy_U+NF_U}{r_p}\right)\cdot V_U+P_{UM}\cdot V_{UM}+\left(P_S+\frac{Phy_S+NF_S}{r_p}\right)\cdot V_S+P_I\cdot V_I+P_D\cdot V_D}{V_U+V_{UM}+V_S+V_I+V_D}$

**Table 2.** $\Delta^{14}C$ (in ‰) data from GLODAP used for calibration of the model physical parameters.

| Box | Lat (S) | Lon (W) | Depth (m) | Data[a] |
|-----|---------|---------|-----------|---------|
| U | 5–15 | 80–90 | 0–100 | −72.39 |
| UM | 5–15 | 80–90 | 100–500 | −93.28 |
| S | 0–20 | 90–190 | 0–100 | −62.21 |
| I | 0–20 | 90–190 | 100–500 | −81.02 |
| D | 0–20 | 80–190 | 500–2000 | −160.30 |
| SI[b] | 20–40 | 90–190 | 100–500 | −71.02 |
| SD[b] | 20–40 | 80–190 | 500–2000 | −134.4 |

[a] GLODAP natural $^{14}C$ data averaged over the respective regions.
[b] SI and SD represent the southern boundary outside the I and D boxes, respectively.

**Table 3.** Summary of model configurations.

| Configuration | Abbreviation | Quadratic mortality | Reduced denitrification rate | $O_2$, $^{14}C$ ventilation of D | $O_2$, $^{14}C$ ventilation of I | $NO_3^-$, $PO_4^{3-}$ exchange of D and I |
|---|---|---|---|---|---|---|
| Standard | STD | | | | | |
| Quadratic-mortality | QM | + | | | | |
| Reduced-denitrification | RD | + | + | | | |
| Ventilation-D | VD | + | | + | | |
| Ventilation-D + Reduced-denitrification | VDRD | + | + | + | | |
| Ventilation-ID | VID | + | | + | + | |
| Ventilation-ID + Reduced-denitrification | VIDRD | + | + | + | + | |
| Open-boundary | OB | + | | + | + | + |
| Open-boundary + Reduced-denitrification | OBRD | + | + | + | + | + |

+ means that the modification applies to this configuration.

**Table 4.** Parameters of the physical model configurations.

| Configuration | STD | VD<br><br>VDRD | VID<br>VIDRD<br>OB<br>OBRD | Units |
|---|---|---|---|---|
| $K_{US}$ | 8.44 | 3.37 | 3.41 | $m\,yr^{-1}$ |
| $K_{UM}$ | 1.59 | 0.40 | 0.58 | $m\,yr^{-1}$ |
| $K_{H}$ | 47 799 | 50 475 | 42 938 | $m\,yr^{-1}$ |
| $A$ | 7.20 | 7.30 | 7.22 | $m\,yr^{-1}$ |
| $B$ | 18.01 | 19.60 | 23.07 | $m\,yr^{-1}$ |
| $g_{U}$ | 9.87 | 8.89 | 9.88 | $m\,yr^{-1}$ |
| $g_{S}$ | 2.94 | 1.42 | 1.46 | $m\,yr^{-1}$ |

**Table 5.** Model parameters.

| Parameter | Description | Units | Value | Range[(reference)] |
|---|---|---|---|---|
| $r_a$ | $O_2$-used/$NO_3$-produced during organic carbon(OC) oxidation | – | 10.6 | 8.6–10.6[a] |
| $r_c$ | C/N ratio of OC oxidation | – | 6.63 | 6.63–7.31[a] |
| $f_U$ | Remineralization ratio in U | – | 20 % | [b] |
| $f_S$ | Remineralization ratio in S | – | 20 % | [b] |
| $f_{UM}$ | Remineralization ratio in UM | – | 70 % | [b] |
| $f_I$ | Remineralization ratio in I | – | 70 % | [b] |
| $r_{den}$ | OC/$NO_3^-$ in denitrification | – | 1.02 | 1.02[a] |
| $r_p$ | N/P released in OC oxidation | – | 16 | 15–16[a] |
| $\mu$ | Maximum growth rate of Phy | $yr^{-1}$ | 91.5 | 36.5–1861.5[c] |
| $\mu_{NF}$ | Maximum growth rate of NF | $yr^{-1}$ | 30.5 | 65.7–438[d] |
| $M$ | Linear grazing-mortality | $yr^{-1}$ | 25 | 40.15–299[e] |
| $M_q$ | Quadratic mortality | $yr^{-1} (\mu mol\, N\, kg^{-1})^{-1}$ | 18.25 | 3.65–18.25[f] |
| $N_h$ | Nitrate half saturation constant | $\mu mol\, N\, kg^{-1}$ | 0.5 | 0.5[g] |
| $P_h$ | Phosphate half saturation constant | $\mu mol\, P\, kg^{-1}$ | 0.03125 | 0.03[h] |
| $L_x$ | Length of box $x$ | m | see Fig. 1 | –confirm |
| $H_x$ | Depth of box $x$ | m | see Fig. 1 | – |
| $K_H$ | Horizontal exchange | $m\, yr^{-1}$ | [l] | 157.68–56 765[a] |
| $K_{US}$ | Vertical mixing between surface and intermediate depth | $m\, yr^{-1}$ | [l] | 0.79–31.54[a] |
| $K_{UM}$ | Vertical mixing between intermediate depth and deep ocean | $m\, yr^{-1}$ | [l] | 0.21–7.88[a] |
| $A + B$ | Upwelling rates | $m\, yr^{-1}$ | [l] | 23.7–630.7[a] |
| $O_{2U}$ | Oxygen concentration in U | $\mu mol\, kg^{-1}$ | 159.54[i] | – |
| $O_{2S}$ | Oxygen concentration in S | $\mu mol\, kg^{-1}$ | 198.11[i] | – |
| $g_U$ | Gas exchange coefficient for U | $m\, yr^{-1}$ | [l] | – |
| $g_S$ | Gas exchange coefficient for S | $m\, yr^{-1}$ | [l] | – |
| $\lambda$ | Radioactive decay rate for $^{14}C$ | $yr^{-1}$ | $1.21 \times 10^{-4}$ | $1.21 \times 10^{-4}$ [j] |
| $N_{DS}$ | Southern boundary nitrate concentration at depth of D | $\mu mol\, N\, kg^{-1}$ | 32.65 | [k] |
| $N_{IS}$ | Southern boundary nitrate concentration at depth of I | $\mu mol\, N\, kg^{-1}$ | 10.93 | [k] |
| $P_{DS}$ | Southern boundary phosphate concentration at depth of D | $\mu mol\, N\, kg^{-1}$ | 2.30 | [k] |
| $P_{IS}$ | Southern boundary phosphate concentration at depth of I | $\mu mol\, N\, kg^{-1}$ | 0.84 | [k] |
| $O_{2DS}$ | Southern boundary phosphate concentration at depth of D | $\mu mol\, N\, kg^{-1}$ | 181.37 | [k] |
| $O_{2IS}$ | Southern boundary phosphate concentration at depth of I | $\mu mol\, N\, kg^{-1}$ | 217.98 | [k] |

[a] Ranges for $r_a$, $r_c$, $r_{den}$, $K_{US}$, $K_{UM}$, $K_H$, $A$ and $B$ are the same as in Canfield (2006).
[b] The fraction of regeneration above 500 m has been estimated between 92 % (Suess, 1980) and 97 % (Martin et al., 1987). According to Canfield (2006), most likely 60–70 % of the export production is remineralised in the OMZ. Thus, we define 20 % and 70 % of export production remineralised in the surface boxes and intermediate boxes respectively.
[c] Furnas (1990)
[d] Robarts and Zohary (1987); Capone et al. (1997)
[e] Caron and Dennett (1999)
[f] Palmer and Totterdell (2001); Schmittner et al. (2008)
[g] Eppley et al. (1969)
[h] McAllister et al. (1964)
[i] Average 0–100 m $O_2$ concentrations of the corresponding areas from World Ocean Atlas (2009).
[j] Libby (1956)
[k] Averages of the corresponding areas from World Ocean Atlas (2009).
[l] These parameter values are defined in Table 4.

**Table 6.** Fluxes comparison with other models. Export production is the export production sinking into the OMZ; aerobic and anaerobic remineralization represent organic matter remineralization under oxic and anoxic conditions respectively; fixed-N loss defines the fixed-N removal from OMZ via denitrification/anammox; input via transport denotes the fixed-N influx into the OMZ from adjacent regions.

| Fluxes ($\mu$mol N kg$^{-1}$ yr$^{-1}$) | Kalvelage et al. (2013) | Mills and Arrigo (2010) | OBRD configuration |
|---|---|---|---|
| Export production | 1.46 | * | 2.25 |
| Aerobic remineralization | 1.00 | * | 1.35 |
| Anaerobic remineralization | 0.45 | * | 0.12 |
| Fixed-N loss | 1.32 | 0.29 | 0.80 |
| Input via transport | 11.41 | * | 1.02 |

* information not available

Title Page

Abstract | Introduction

Conclusions | References

Tables | Figures

|◄ | ►|

◄ | ►

Back | Close

Full Screen / Esc

Printer-friendly Version

Interactive Discussion

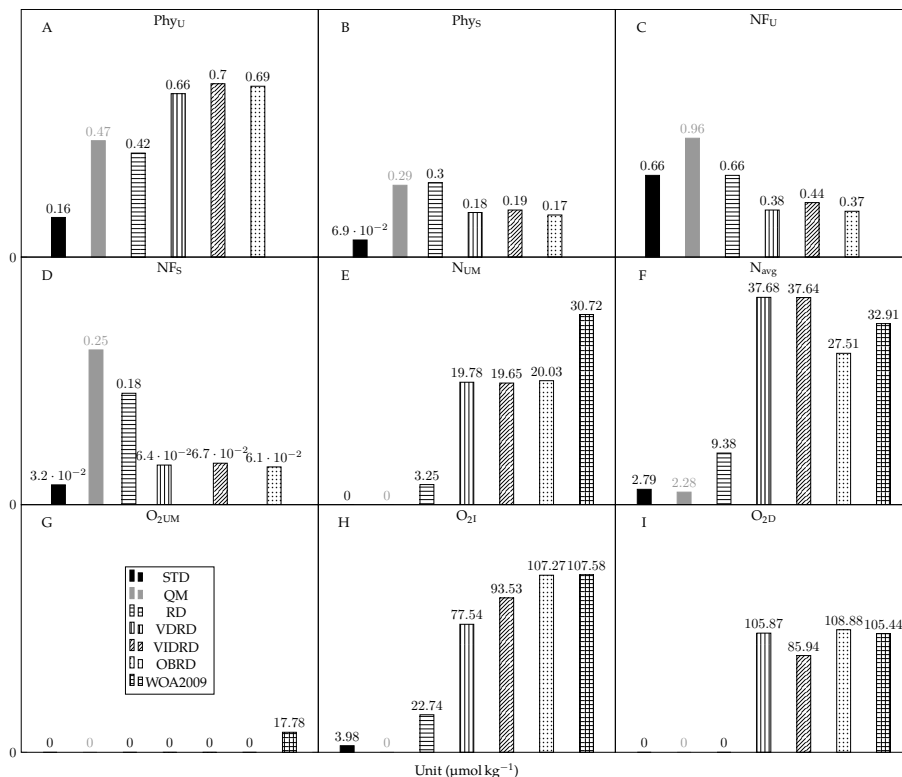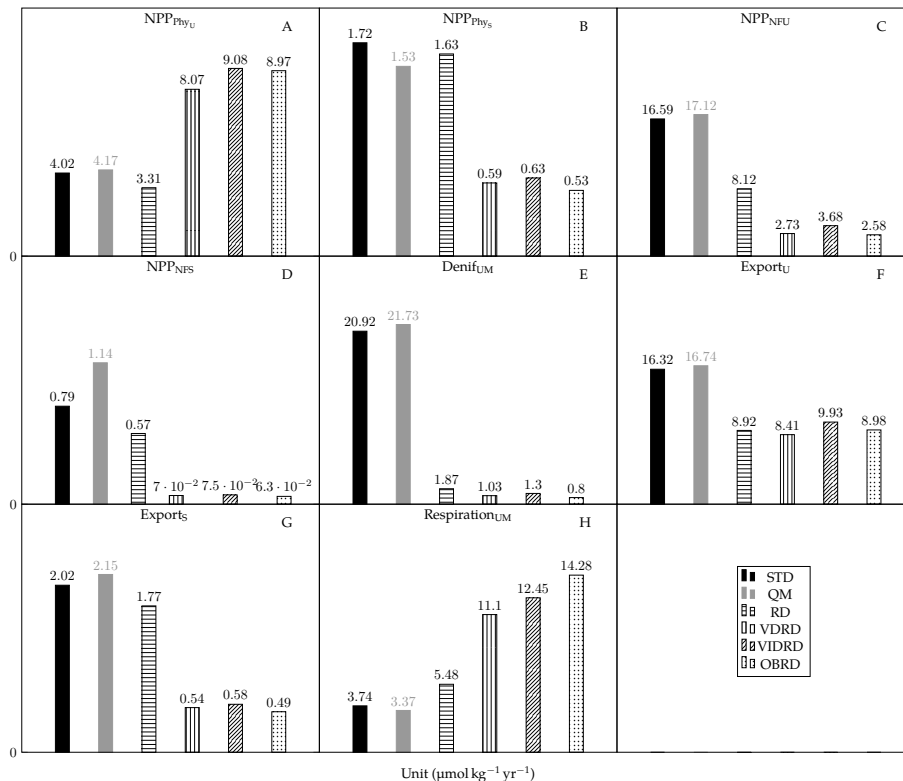**What prevents nitrogen depletion in the OMZ of the Eastern Tropical South Pacific?**

B. Su et al.
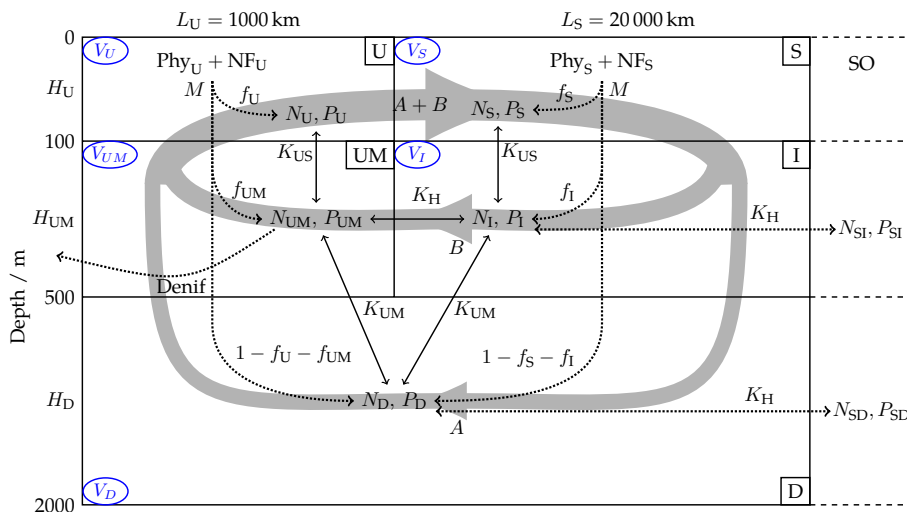
**Figure 1.** Model structure and configurations. The model domain comprises five active boxes representing the top 100 m of an upwelling region (U), the underlying oxygen minimum zone (UM), and an adjacent open-ocean basin divided into a surface (S) and an intermediate-depth box (I). A deep box (D) underlies both the upwelling region and the open ocean. The large-scale circulation is represented by deep ($A$) and shallow ($B$) convection (thick grey lines). Mixing between boxes is implemented via mixing coefficients ($K$). Remineralization derived from net primary production by ordinary (Phy) and diazotrophic (NF) phytoplankton in the surface boxes consumes oxygen. Under anoxic conditions remineralization is fueled by anaerobic remineralization (Denif). The model can be configured to exchange nutrients and oxygen with the southern subtropical ocean (right). See Table 5 for symbol definitions and text for details.

**Figure 2.** Simulated steady-state phytoplankton, nutrient and oxygen concentrations for the model configurations defined in Tables 3 and 4. Each panel uses linear scale of the y-axis starting at zero. Gridded panels represent the average of the WOA2009 data of the corresponding boxes, however, there are no data for $Phy_U$, $Phy_S$, $NF_U$ and $NF_S$.

**Figure 3.** Simulated steady-state biogeochemical fluxes for the model configurations defined in Tables 3 and 4. $NPP_{PhyU}$, $NPP_{PhyS}$, $NPP_{NFU}$ and $NPP_{NFS}$ represent the net primary production rates of $Phy_U$, $Phy_S$, $NF_U$ and $NF_S$ respectively. $Denif_{UM}$ indicates the nitrogen loss rate by anaerobic remineralization in the UM box. $Export_U$ and $Export_S$ represent the export production rate out of U and S. $Respiration_{UM}$ represents aerobic respiration rate in the UM box. Note that all panels are in units of nitrogen except **(H)**, which is in units of $O_2$. Each panel uses a differrent linear scale for the y-axis starting at zero.

Title Page

Abstract | Introduction

Conclusions | References

Tables | Figures

|◄ | ►|

◄ | ►

Back | Close

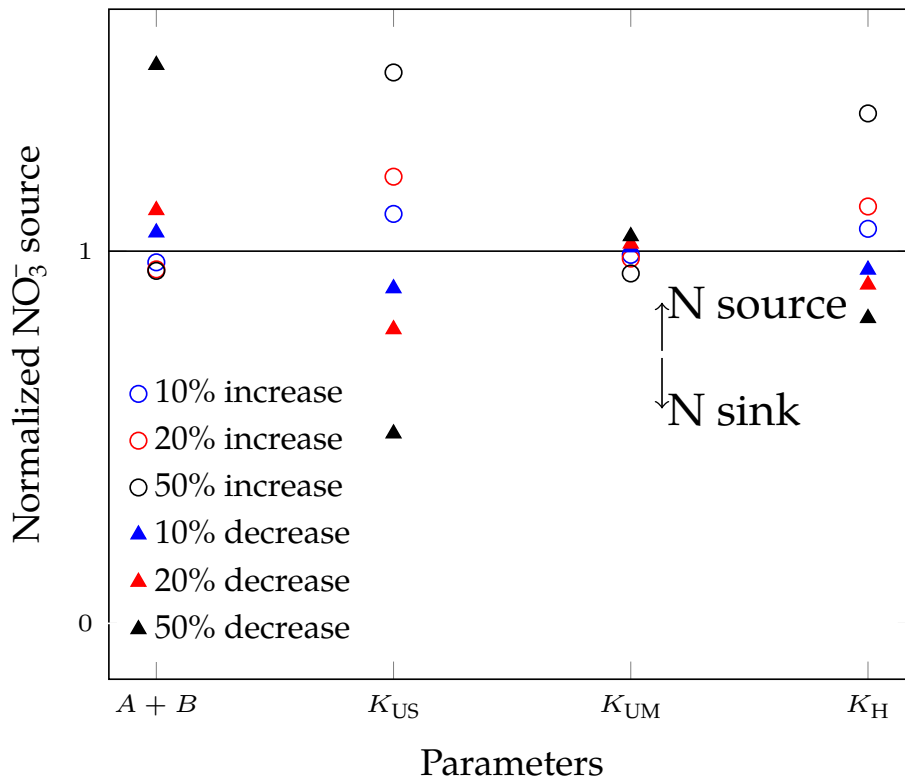Full Screen / Esc

Printer-friendly Version

Interactive Discussion

Full Screen / Esc

Printer-friendly Version

Interactive Discussion
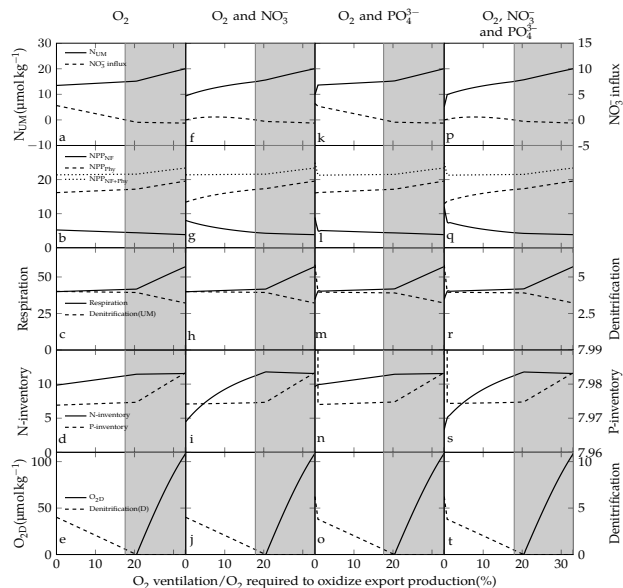


**Figure 4.** Dependence of the biogeochemical processes on the ratio of $O_2$ supply from the subtropical ocean and export production from the surface ocean (boxes U and S). $N_{UM}$ and $NO_3^-$ influx represent $NO_3^-$ concentration in the UM box and $NO_3^-$ flux from the southern boundary (positive into model domain). $NPP_{Phy}$, $NPP_{NF}$ and $NPP_{NF+Phy}$ are net primary production by ordinary phytoplankton, nitrogen fixers, and the sum of ordinary phytoplankton and nitrogen fixers in surface ocean. Respiration and denitrification (UM) represent $O_2$ consumption by aerobic remineralization and $NO_3^-$ removal by anaerobic remineralization, respectively, in the UM box. N-inventory and P-inventory are the total nitrogen and phosphorus inventories in the model domain, including all the related organic and inorganic species. $O_{2D}$ and denitrification (D) represent $O_2$ concentration and $NO_3^-$ removal by anaerobic remineralization in the D box. Units of all the variables in this figure are $10^{11}$ $\mu mol\,yr^{-1}\,m^{-1}$ except for $N_{UM}$ and $O_{2D}$, which are given in $\mu mol\,kg^{-1}$. The shaded area denotes the parameter range for which the model domain is a net source of fixed-N.

**Figure 5.** Sensitivity of the strength of the net $NO_3^-$ flux out of the model domain for different variations of the individual parameters describing ocean transport (see Table 4 and Fig. 1 for a description of the parameters). The flux is normalized by the flux simulated by the OBRD model configuration.

Full Screen / Esc

Printer-friendly Version

Interactive Discussion
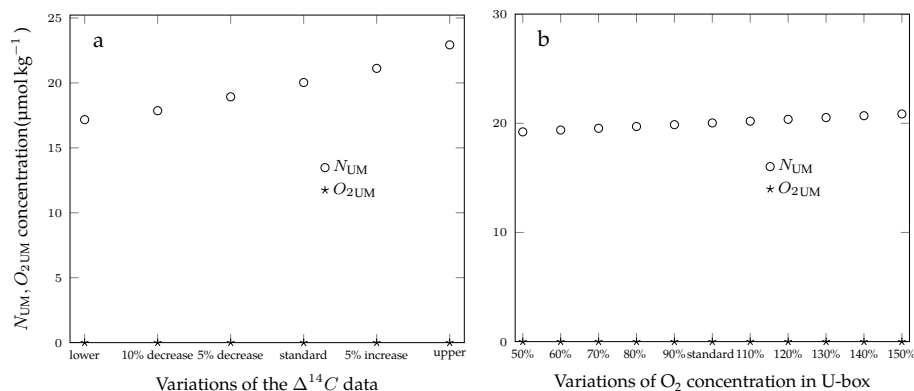
**Figure 6.** $NO_3^-$ and $O_2$ concentrations in the OBRD configuration for different physical parameters derived from variations of the $\Delta^{14}C$ data **(a)** and $O_2$ concentration in U-box **(b)**. **(a)** Decrease and increase mean that $\Delta^{14}C$ values in all boxes are reduced or increased simultaneously. **(b)** Values of the x-axis denote the variations of $O_2$ concentration in the U-box relative to the standard. Standard run in each figure is the OBRD configuration with physical parameters defined in Table 4.
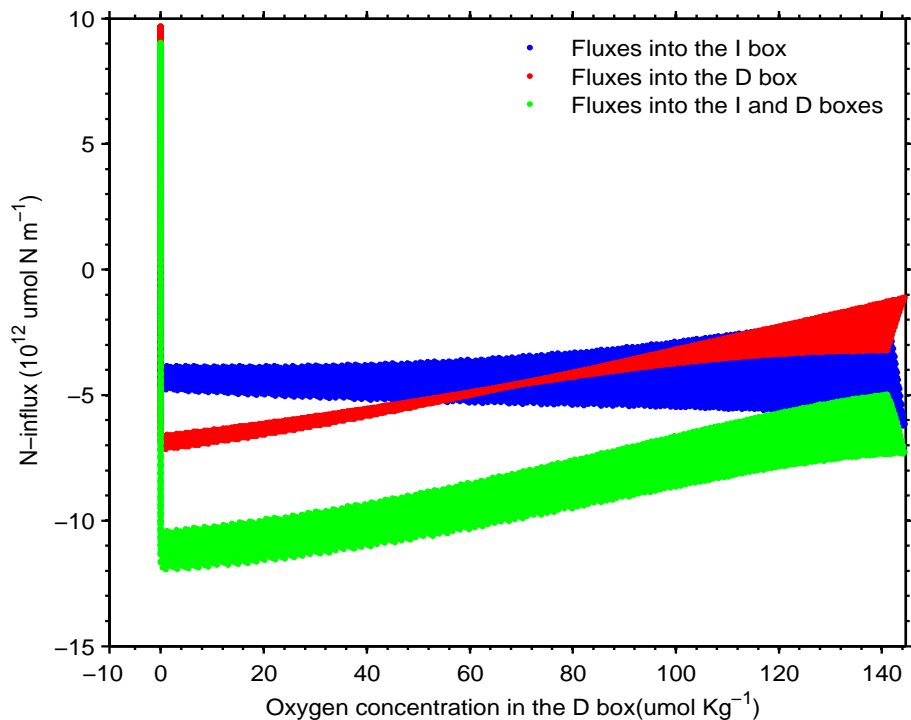
**Figure 7.** Lateral $NO_3^-$ input into the model domain of the OBRD configuration. "Fluxes into the I box" represents lateral $NO_3^-$ input into the I box; "fluxes into the D box" represents lateral $NO_3^-$ input into the D box; "fluxes into the I and D boxes" is the sum of the above two processes. In this figure, negative values indicate that the model is a $NO_3^-$ source, and positive values that the model is a $NO_3^-$ sink instead.
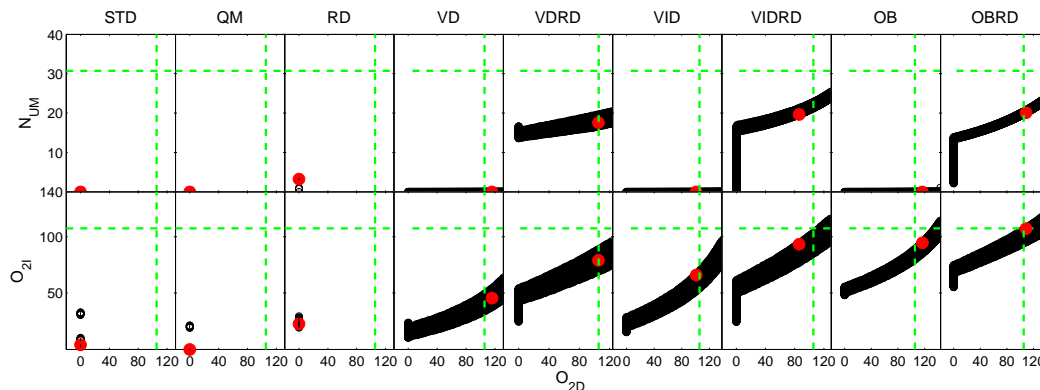
**Figure 8.** $NO_3^-$ concentration in the OMZ and $O_2$ concentrations in the I box for all combinations of physical transport parameters in the literature range. The x-axis is the $O_2$ concentration in the D box. Red dot in each panel is the selected suite of physical transport parameters which fit the biogeochemical data best in each model configuration. The horizontal green dashed lines represent the average of WOA2009 data for $N_{UM}$ and $O_{2I}$, and the vertical green dashed lines denote the average of WOA2009 data for $O_{2D}$.
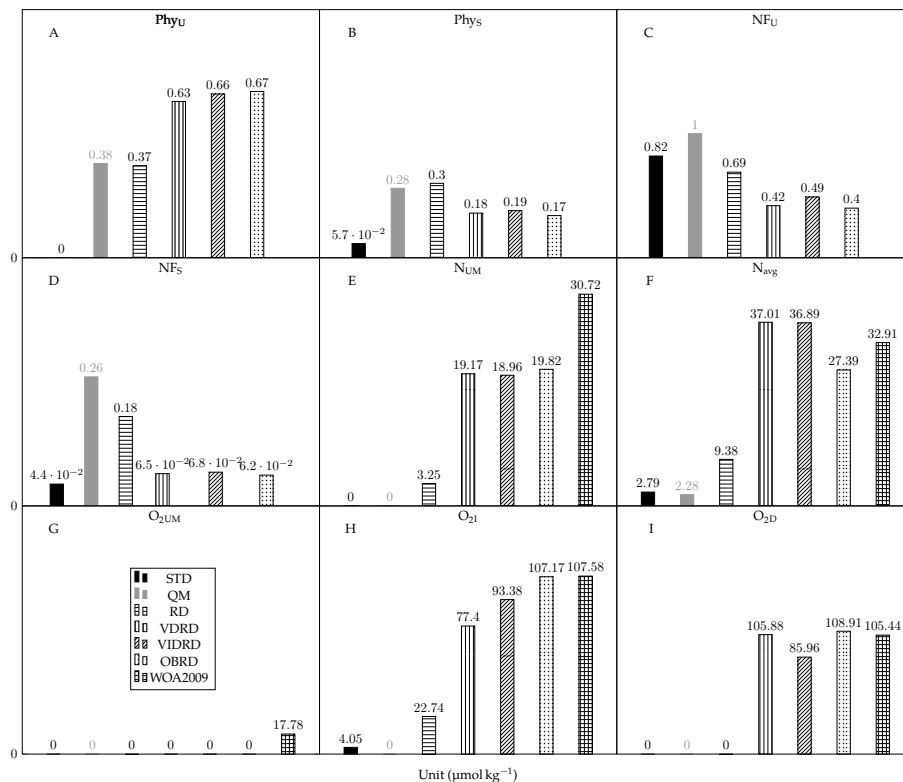
**Figure 9.** Same as Fig. 2 but with diazotrophs utilising also nitrate when available (Eqs. D1 and D2). Again, each panel uses a different linear scale for the y-axis starting at zero. Gridded panels represent the average of the WOA2009 data of the corresponding boxes, however, there are no data for $Phy_U$, $Phy_S$, $NF_U$ and $NF_S$.

Title Page

Abstract | Introduction

Conclusions | References

Tables | Figures

|◄ | ►|

◄ | ►

Back | Close

Full Screen / Esc

Printer-friendly Version

Interactive Discussion